CHALMERS
UNIVERSITY OF TECHNOLOGY

Aerodynamic Analysis and Cab Geometry Optimization of an Electric Heavy-Duty Truck

Master's thesis in Mobility Engineering

Yazan Najjar

DEPARTMENT OF MECHANICS AND MARITIME SCIENCES

CHALMERS UNIVERSITY OF TECHNOLOGY
Gothenburg, Sweden 2026
www.chalmers.se

Master's thesis 2026

Aerodynamic Analysis and Cab Geometry Optimization of an Electric Heavy-Duty Truck

Yazan Najjar

CHALMERS
UNIVERSITY OF TECHNOLOGY

Department of Mechanics and Maritime Sciences
Chalmers University of Technology
Gothenburg, Sweden 2026

Aerodynamic Analysis and Cab Geometry Optimization of an Electric Heavy-Duty Truck
YAZAN NAJJAR

Supervisor: Chao Xia, Department of Mechanics and Maritime Sciences
Examiner: Simone Sebben, Department of Mechanics and Maritime Sciences

Master's Thesis 2026
Department of Mechanics and Maritime Sciences
Chalmers University of Technology
SE-412 96 Gothenburg
Telephone +46 31 772 1000

Abstract

This thesis investigates the influence of cab geometry and aerodynamic add-ons on the aerodynamic performance of a heavy-duty electric truck using computational fluid dynamics. A parameterized 3D-CAD tractor-trailer model was developed in STAR-CCM+ and evaluated using steady Reynolds-Averaged Navier–Stokes simulations with the SST k-ω turbulence model. Two cab geometries were studied: a baseline flat-front cab and a more streamlined electric-truck cab. For each cab geometry, configurations with a large side skirt and a side extender were simulated to assess the effect of add-ons on the tractor-trailer gap and underbody flow. A two-stage cab optimization was then performed using the SHERPA algorithm, first on a simplified model and then on the complete Model 1 configuration.

The results show that cab geometry has a strong influence on both the front pressure distribution and the effectiveness of the add-ons. For Model 1, the combined large side skirt and side extender reduced the drag coefficient from 0.407 to 0.391, corresponding to a reduction of approximately 3.9%. For the more streamlined Model 2, the same add-on configuration reduced the drag coefficient from 0.411 to 0.364, corresponding to a reduction of approximately 11.4%. The complete Model 1 optimization reduced the drag coefficient from 0.391 to 0.373, giving an additional reduction of approximately 4.6% relative to Model 1 configuration 3. The accumulated drag and pressure-coefficient results indicate that this improvement mainly originates from the optimized cab-front shape, while the downstream flow remains strongly affected by the side skirt, side extender, and trailer arrangement.

The work provides a foundation for continued research on aerodynamic analysis and optimization of zero-emission heavy-duty vehicles. The parameterized model and CFD workflow can be further refined to include additional design concepts, experimental validation, and more realistic operating conditions such as crosswind.

Keywords: electric heavy-duty truck, truck aerodynamics, CFD, aerodynamic add-ons, cab geometry optimization.

Acknowledgments

I would like to express my sincere gratitude to my supervisor, Chao Xia, and my examiner, Simone Sebben, for their guidance and support throughout this project. I am thankful to Chao for his continuous availability, patience, and the valuable time he dedicated to helping me during this study. His feedback and guidance were greatly appreciated. I would also like to thank Simone for giving me the opportunity to undertake this study and for her encouragement throughout the process.

Yazan Najjar, Gothenburg, June 2026

List of Acronyms

Below is the list of acronyms that have been used throughout this thesis listed in alphabetical order:

BEV	Battery Electric Vehicle
CAD	Computer-Aided Design
CFD	Computational Fluid Dynamics
FCV	Fuel Cell Vehicle
IDDES	Improved Delayed Detached Eddy Simulation
RANS	Reynolds-Averaged Navier–Stokes
ZEHDV	Zero Emission Heavy Duty Vehicles
ZEV	Zero Emission Vehicles

Contents

List of Figures

List of Tables

1
Introduction

The transition toward zero-emission heavy-duty vehicles (ZEHDVs) is reshaping the design priorities of freight transport. For electric heavy-duty trucks, energy efficiency is directly linked to driving range, battery utilization, and operational feasibility. Emerging ZEHDV concepts are already showing shape changes associated with improved aerodynamic performance, including smaller cooling-air inlets, angled windshields, and larger corner radii. Wind-tunnel tests of a zero-emission cab shape showed a 7–9% reduction in aerodynamic drag compared with a conventional cab reference [1]. This makes aerodynamic design a central part of evaluating future electric heavy-duty truck concepts.

(a) Scania

(b) Volvo

(c) Tesla Semi

(d) Windrose

Figure 1.1: Cab-front designs of conventional cab-over trucks and emerging electric heavy-duty trucks

Figure 1.1 highlights how electrification changes the aerodynamic design space for heavy-duty truck cabs. Conventional cab-over tractors, represented here by Scania and Volvo examples, are strongly influenced by diesel-powertrain packaging, radiator and intercooler requirements. Electric heavy-duty concepts such as the Tesla Semi and Windrose tractor can redistribute cooling and powertrain components, which

permits a more continuous cab nose, reduced grille area, smoother windshield-to-roof transitions, and larger front corner radii. These geometric differences do not automatically guarantee lower drag for a complete tractor-trailer combination, but they make the electric-truck cab shape a particularly important target for aerodynamic investigation.

Regulatory changes also support this design shift. Recent amendments to European Union regulations on the maximum authorized dimensions and weights of heavy-duty vehicles aim to facilitate the adoption of zero-emission technologies. According to the Council of the European Union, the updated directive introduces allowances for additional vehicle mass and limited extensions in vehicle length, provided that these measures contribute to improved aerodynamic performance without reducing cargo capacity [2].

Aerodynamic efficiency is especially important at highway speeds, where aerodynamic drag becomes a major part of the power demand. For electric heavy-duty vehicles, reducing drag can lower energy consumption, extend driving range, and reduce the battery energy required for long-distance operation. A review of aerodynamic drag-reduction devices for heavy trucks estimated that a 20% reduction in drag can reduce fuel consumption by about 10% at 80 km/h and by approximately 15% at 120 km/h [3]. This illustrates why aerodynamic design remains important for both conventional and zero-emission heavy-duty vehicles.

This thesis develops and parameterizes a standardized reference model of an electric heavy-duty truck, including the tractor, trailer, and wheel configuration, and uses this model to investigate its aerodynamic performance. The study combines parametric geometry development and computational fluid dynamics (CFD) simulations to evaluate how cab geometry, aerodynamic add-ons, and cab-shape optimization influence aerodynamic drag.

1.1 Research Objectives

The objectives of this project are to:

- Design and parameterize a 3D CAD geometry of a reference electric truck model, including tractor, trailer, and wheel configuration.
- Conduct CFD simulations on the model to assess the impact of selected aerodynamic design features, including cab geometry and aerodynamic add-ons such as side extenders and side skirts, on the aerodynamic drag of the truck.
- Perform cab geometry optimization using the SHERPA algorithm with the objective of reducing aerodynamic drag.

1.2 Limitations

A limitation of this project is the absence of experimental validation through wind tunnel testing due to time and resource constraints. The study therefore depends

on computational methods to evaluate the aerodynamic performance of the models.

The simulations are limited to a yaw angle of 0°, representing straight-forward driving without crosswind effects. The study focuses on aerodynamic performance and does not evaluate cost, structural integrity, durability, manufacturing constraints, or operational aspects such as loading, maintenance, and maneuverability.

1.3 Outline

Chapter 2 presents the environmental motivation and literature background for heavy-duty vehicle aerodynamics. Chapter 3 describes the truck model, CFD setup, and optimization method. Chapter 4 evaluates the aerodynamic effects of add-ons and cab geometry. Chapter 5 presents the cab optimization results. Chapter 6 summarizes the main conclusions and suggests further work.

2
Background

This chapter presents the environmental motivation for aerodynamic improvement, reviews previous research on generic truck models and aerodynamic optimization, and summarizes the main findings that guide the present work.

2.1 Environmental Aspects

Road transport is a major contributor to greenhouse gas emissions in the European Union. The European Commission reports that road transport accounts for about one quarter of total EU greenhouse gas emissions, while heavy-duty vehicles, including lorries, buses, and coaches, are responsible for more than a quarter of road transport greenhouse gas emissions and for over 6% of total EU greenhouse gas emissions [4, 5]. Reducing the energy demand of trucks is therefore directly connected to reducing the environmental impact of freight transport. At steady speed on level road, the resistive force that must be overcome can be approximated as the sum of aerodynamic drag and rolling resistance, $F_{\mathrm{res}} = F_{\mathrm{d}} + F_{\mathrm{rr}} = \frac{1}{2}\rho C_{\mathrm{d}} A_{\mathrm{f}} v^2 + C_{\mathrm{rr}} mg$, and the required propulsion power is $P_{\mathrm{req}} = F_{\mathrm{res}} v$. This means that the aerodynamic power demand increases with the cube of vehicle speed, while rolling-resistance power increases approximately linearly with speed. Consequently, reducing aerodynamic drag is especially important at highway speeds and can improve the range and energy efficiency of zero-emission heavy-duty vehicles.

2.2 Literature Review

2.2.1 Generic Truck Aerodynamic Model

Generic truck aerodynamic models are widely used because they provide controlled geometries for studying heavy-vehicle flow physics and for validating numerical methods. Full production trucks contain many small details, such as mirrors, cooling openings, suspension components, and underbody structures, which make it difficult to isolate the aerodynamic mechanisms responsible for drag. Simplified models therefore provide a common reference geometry where wind tunnel measurements and CFD simulations can be compared consistently.

The Generic Conventional Model (GCM) is one of the most important examples of a realistic but simplified tractor-trailer model. Storms et al. [6] summarized wind tunnel measurements of the GCM in the NASA Ames 7- by 10-Foot Wind Tunnel

and the 12-Foot Pressure Wind Tunnel. The 1:8-scale model retained the main features of a conventional Class 8 tractor-trailer while simplifying the underbody and removing small-scale details to support computational modeling. The experimental database included component forces and moments, surface pressures, dynamic pressure measurements, and three-component particle image velocimetry. The tests also examined several drag-reduction concepts, making the GCM a useful benchmark for studying both baseline truck aerodynamics and add-on devices.

The GCM has also been used in numerical studies. Sreenivas et al. [7] performed aerodynamic simulations of the GCM and compared the computed forces and pressure coefficients with NASA Ames wind tunnel data at different yaw angles. Their study showed that numerical simulations can reproduce important trends in the measured aerodynamic forces, while also highlighting the sensitivity of pressure prediction to mesh resolution and turbulence modeling. This makes the GCM valuable not only as an experimental model, but also as a validation case for high-fidelity CFD methods applied to tractor-trailer aerodynamics.

Another widely used benchmark is the Ground Transportation System (GTS) model. Compared with the GCM, the GTS is a more idealized cab-over-engine tractor-trailer geometry without wheels and without a tractor-trailer gap, which makes it suitable for studying separated flow, base wake behavior, and simplified drag-reduction concepts. Storms et al. [8] tested a 1:8-scale GTS model in the NASA Ames 7- by 10-Foot Wind Tunnel and measured drag, surface pressures, hot-film data, oil-film interferometry, and three-dimensional PIV. Boattail plates were also tested at the trailer rear, providing a clear geometry modification for evaluating wake-control strategies.

The GTS has been extensively used for CFD validation. Roy et al. [9] conducted steady RANS simulations of a simplified tractor-trailer geometry and compared vehicle drag, surface pressure, and near-wake velocity predictions with NASA Ames wind tunnel data. The results showed that RANS methods could capture much of the surface pressure distribution, but that the trailer base wake remained difficult to predict accurately. Later, Roy and Ghuge [10] applied Detached Eddy Simulation to the same type of simplified tractor-trailer flow and reported improved drag prediction on finer grids while still noting challenges in resolving the turbulent near wake. These studies show why the GCM and GTS remain widely used as they provide repeatable experimental databases, clear geometry definitions, and benchmark cases for assessing turbulence models, mesh strategies, and drag-reduction concepts in truck aerodynamics.

2.2.2 Truck Aerodynamics and Optimization

Research on heavy-duty vehicle aerodynamics generally identifies several coupled regions that dominate the aerodynamic performance of a tractor-trailer combination: the cab, the tractor-trailer gap, the trailer underbody and bogie region, and the trailer base wake. Previous work on commercial vehicle drag reduction shows

that improvements are therefore not limited to smoothing the tractor front. They also depend on controlling separated flow and pressure losses around the gap and trailer add-on devices [11, 12]. This interaction is especially relevant for the present study, where cab geometry, side extenders, and side skirts are evaluated as parts of the same vehicle system.

The tractor-trailer gap is one of the most important regions for add-on devices. Flow leaving the tractor rear surfaces can enter the gap, form recirculation, and impinge on the trailer front, increasing pressure losses and unsteady vortical structures. Gap fairings, and side extenders are used to guide the flow and reduce the exchange of high-momentum external flow with the separated gap region. Kim et al. [13] investigated gap fairings through wind-tunnel tests and particle image velocimetry on a scaled tractor-trailer model. Their proposed gap fairing reduced drag by up to 16.4%, while aero cab fairing concepts combining cab-roof and gap-fairing effects reduced the drag coefficient by approximately 11.1% to 17.5%. The study also showed reductions in mean velocity, vorticity, and turbulent kinetic energy in the gap region, explaining why controlling the tractor-trailer gap can significantly reduce the aerodynamic load on the trailer front.

Side skirts address a different but coupled loss mechanism associated with the trailer underbody. The open underbody allows flow to interact with wheels, bogie structures, and ground clearance, generating vortical activity and momentum loss. Hwang et al. [14] showed that side skirts can reduce drag by more than 5% by shielding the underbody flow and reducing the interaction between the external flow, rotating wheels, and structural components. This indicates that underbody devices are most effective when they restrict cross-flow and prevent energetic flow from entering the region beneath the trailer. Full-scale wind-tunnel work by Ortega et al. [15] further demonstrated that combining several aerodynamic add-ons can provide cumulative drag-reduction benefits, meaning that gap treatments and side skirts should be assessed as part of the complete tractor-trailer configuration rather than as isolated devices.

Optimization studies build on this device-based understanding by using CFD and parameterized geometry changes to search a larger design space. In truck aerodynamics, optimization commonly focuses on cab curvature, windshield angle, roof and side fairings, side extenders, side skirts, and other add-on configurations, while the drag coefficient is used as the primary response variable. Prabhu et al. [16] reported an 18% drag reduction through CFD-based design optimization of a commercial vehicle, demonstrating the potential of numerical optimization for truck aerodynamic design. Studies on next-generation truck design also suggest that an improved tractor shape does not guarantee the best complete vehicle performance unless its interaction with the trailer, underbody, and wake is considered [1]. These findings motivate the present work, in which cab geometry, add-on devices, and optimization are evaluated together for an electric heavy-duty truck concept.

2.2.3 Summary of Findings

The existing studies provide valuable insights, but they are limited by the variety of models. Most generic aerodynamic models and add-ons are tested with conventional truck designs. However, the recent shift toward zero-emission heavy-duty vehicles opens up new design possibilities. Developing and evaluating emerging truck models is important because it provides a better understanding of their aerodynamic potential, which can lead to more efficient and optimized truck designs in the future.

3

Methodology

This chapter describes the truck design process, the CFD simulation setup, and the optimization setup in STAR-CCM+.

3.1 Truck Model

The electric heavy-duty truck geometry was constructed as a parameterized 3D-CAD model in STAR-CCM+. The model was designed so that the main cab shape variables could be modified while the trailer, wheel layout, and other reference components remained consistent between comparable cases. This made it possible to evaluate the aerodynamic effect of individual geometry changes and later use the same model structure for optimization.

The complete vehicle model represents a tractor-trailer combination. The tractor cab is the primary design region in this thesis because the cab front, windshield, roof transition, side corners, and tractor-trailer gap strongly influence the incoming flow and the pressure distribution on the vehicle. The trailer and wheels were included to preserve the main flow interactions of an on-road heavy-duty truck, especially the underbody flow and the wake generated by the tractor-trailer combination.

The 3D-CAD model was controlled through a set of geometric parameters, as illustrated in Figure 3.1. These parameters define the main cab, including the roof angle, side angle, windshield angle, fender angle, bumper height, cab length, and several radii controlling the windshield-roof transition, fenders, bumper, and front side corners. Using named parameters in the CAD model allowed the same modeling procedure to generate both the baseline cab and the more streamlined cab geometry.

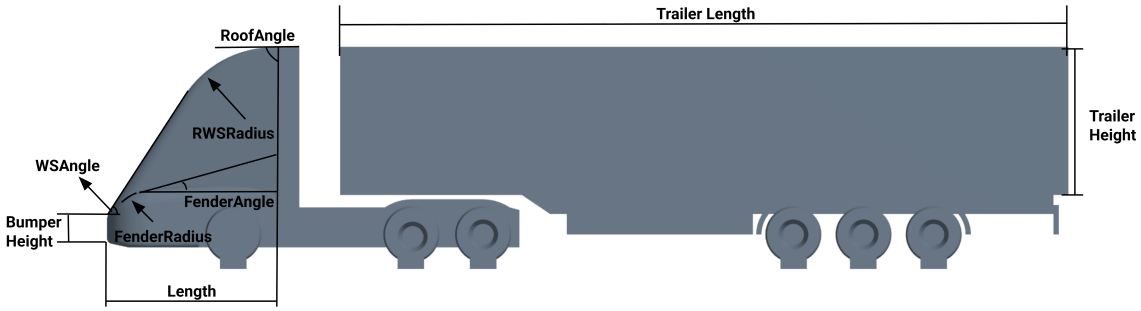

(a) Side view of the truck

(b) Top and bottom view of the tractor

Figure 3.1: The parameters used to create the truck

Table 3.1: The parameters used to create the models

Parameter	Model 1	Model 2
RoofAngle (deg)	89	89
SideAngle (deg)	5	10
WSAngle (deg)	80	60
FenderAngle (deg)	10	3
BumperHeight (m)	1.25	0.6
FilletRadius (m)	0.2	0.3
RWSRadius (m)	0.5	2
FenderRadius (m)	0.2	1.1
BumperRadius (m)	0.2	0.75
SideRadius (m)	0.215	0.3
Length (m)	2.26	3.2
Trailer Length (m)	13.7	13.7
Trailer Height (m)	2.78	2.78
Track Width (m)	2.45	2.45
Wheelbase (m)	4.15	4.15

Two cab geometries were generated from this parameterized model. Model 1 is the baseline geometry and represents a more conventional flat-front heavy-duty cab. Model 2 was developed to represent the smoother cab shapes seen in emerging electric heavy-duty truck concepts, such as the Tesla Semi. Compared with Model 1,

Model 2 has a lower windshield angle (WSAngle), reduced bumper height, smaller fender angle, longer cab length, and larger radii at the roof-windshield (RWS) transition, fenders, bumper, and front side corners. The parameter values used for the two cab geometries are summarized in Table 3.1.

The configurations were then organized to separate the effects of cab geometry and aerodynamic add-ons. Model 1 configuration 0 is a simplified tractor-trailer model without wheels and detailed underbody components, as shown in Figure 3.2. This simplified configuration was used as an initial optimization case because it reduces computational cost and provides a controlled starting point for testing the cab-shape parameters.

Configurations 1–3 use the complete vehicle representation with wheels and underbody details. Configuration 1 is the reference configuration for each cab geometry. Configuration 2 adds a large side skirt to reduce flow interaction with the trailer-underbody region, and configuration 3 combines the large side skirt with a side extender to reduce the tractor-trailer gap. The side extender and side skirt are highlighted in red in Figures 3.5b and 3.4b. The trailer geometry, wheel layout, track width, and wheelbase are kept identical across the complete configurations so that differences in aerodynamic performance can be attributed to the cab geometry and add-on devices.

Table 3.2: Summary of truck models and configurations

Model	Configuration	Wheels	Large Side Skirt	Side Extender	Purpose
Model 1	Config. 0				Initial optimization
Model 1	Config. 1	x			Reference configuration
Model 1	Config. 2	x	x		Evaluate large side skirt effect
Model 1	Config. 3	x	x	x	Evaluate combined aerodynamic devices
Model 2	Config. 1	x			Reference configuration
Model 2	Config. 2	x	x		Evaluate large side skirt effect
Model 2	Config. 3	x	x	x	Evaluate combined aerodynamic devices

Figure 3.2: Model 1, configuration 0

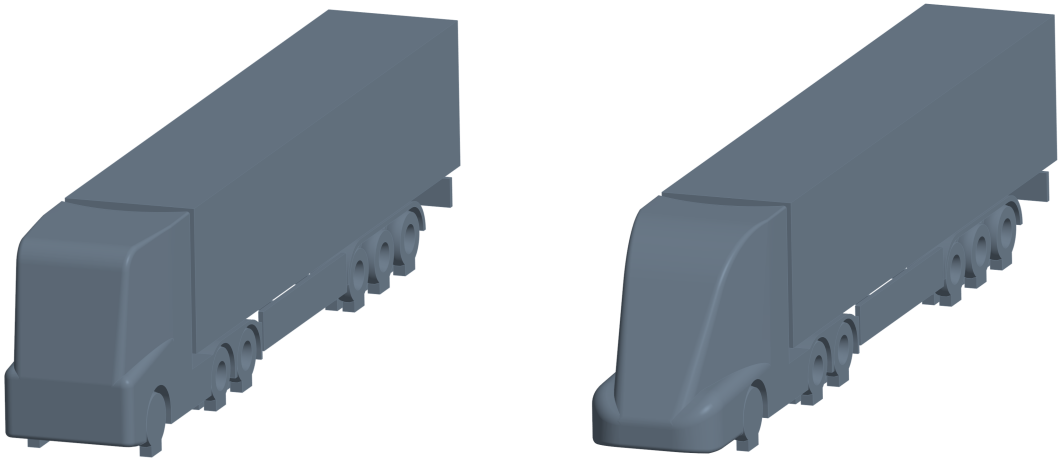

(a) Model 1 **(b)** Model 2

Figure 3.3: Model 1 and Model 2, configuration 3

(a) Configuration 1 **(b)** Configuration 2 and 3

Figure 3.4: Trailer-underbody gap

(a) Configuration 1 **(b)** Configuration 3

Figure 3.5: The tractor-trailer gap

3.2 Numerical Setup

The aerodynamic simulations were carried out in Simcenter STAR-CCM+ version 2506. The numerical setup was defined to evaluate the steady-state aerodynamic performance of the truck models under straight-ahead highway driving conditions.

3.2.1 Physics Model

The flow was solved using the Reynolds-Averaged Navier–Stokes (RANS) approach. In RANS simulations, the turbulent flow field is decomposed into mean and fluctuating components, and the governing equations are solved for the mean flow quantities. This approach is widely used in industrial vehicle aerodynamics because it provides a practical balance between computational cost and engineering accuracy [17].

The flow was assumed to be incompressible because the freestream velocity used in this study corresponds to a Mach number below 0.3. Under this condition, density variations are small and the density can be treated as constant. Turbulence was modeled using the SST k-ω model. This model combines the near-wall accuracy of the k-ω formulation with the freestream robustness of the k-ϵ formulation through a blending function [18]. It is suitable for the present heavy-duty truck simulations because separation, near-wall boundary layers, and wake formation are important contributors to aerodynamic drag. A coupled flow solver was used to improve convergence behavior.

3.2.2 Computational Domain

The computational domain was built to represent the flow around the truck in open-road conditions. The domain is three-dimensional and includes a velocity inlet at the upstream face, a pressure outlet at the downstream face, and symmetry-plane conditions on the top and side boundaries. The domain is illustrated in Figure 3.6.

At the inlet, a freestream velocity of 25 m/s was applied, corresponding to typical highway driving conditions. The yaw angle was set to 0°, representing straightforward driving without crosswind effects. The outlet was defined as a pressure outlet, allowing the flow to leave the domain with minimal upstream influence. The truck surfaces were treated as no-slip walls.

The ground boundary was divided into two regions. A no-slip ground condition was applied directly under the truck to represent the vehicle-road interaction, where near-wall effects are important. Upstream of the vehicle, a slip ground condition was used to reduce artificial boundary-layer growth before the flow reaches the truck. Wheel rotation was included by applying an angular velocity of 47.4 rad/s, representing realistic rolling conditions and improving the local flow prediction around the wheels.

The coordinate system was defined such that the positive x-direction is aligned with the longitudinal axis of the truck and points toward the rear of the vehicle. The positive y-direction is oriented laterally toward the right-hand side of the truck, and the positive z-direction points upward. The aerodynamic force components were defined using the same coordinate system: drag force in the x-direction, side force in the y-direction, and lift force in the z-direction. The moments about the x-, y-, and z-axes were defined as roll, pitch, and yaw moments, respectively. Each simulation was run for a maximum of 3000 iterations, with convergence assessed from residual behavior and the stabilization of key aerodynamic quantities, especially drag force.

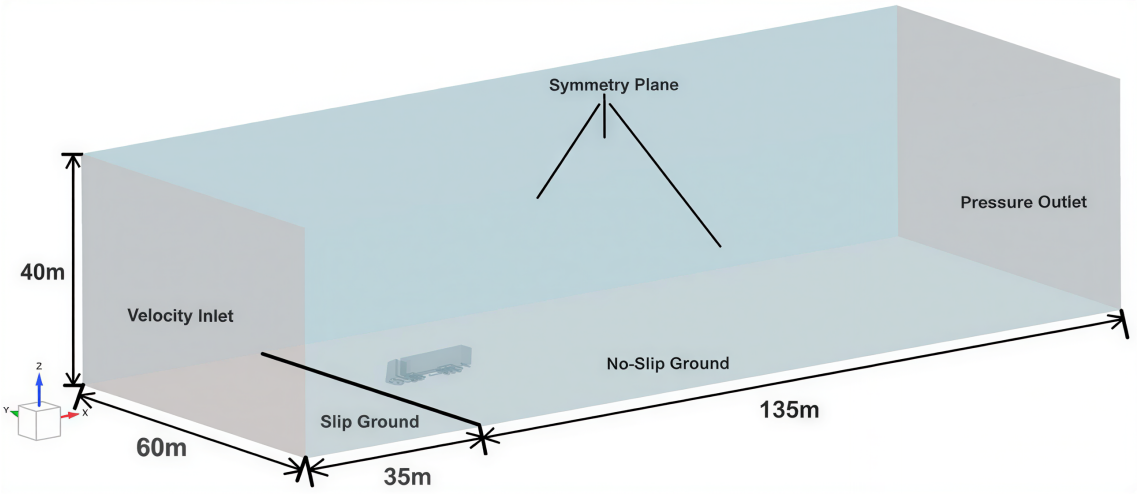

Figure 3.6: The computational domain

3.2.3 Mesh Sensitivity Study

A surface remesher was used to define the surface mesh with the aim of having large cell size near the boundaries of the domain and smaller cell size around the truck, as shown in Figure 3.7. This is done by creating five refinement regions around the truck to reduce computational cost without affecting the accuracy of the simulation. A prism layer mesher was also used to capture the boundary layer formation on the surface of the truck, as shown in Figure 3.8.

A mesh sensitivity study was performed to ensure that the simulation results do not depend on the cell mesh count, as shown in Table 3.3. Three mesh qualities were tested: coarse, medium, and fine. Given that the fine mesh had almost no effect on the drag coefficient (C_d) and lift coefficient (C_l), and considering the computational expense associated with further increasing mesh resolution, the resolution of the medium mesh was regarded as sufficient. All results presented in this thesis are based on the medium mesh.

Table 3.3: Mesh sensitivity study

	Coarse	**Medium**	**Fine**
Cd	0.407	0.407	0.406
Cl	0.468	0.467	0.468
Number of cells (millions)	7	18	31

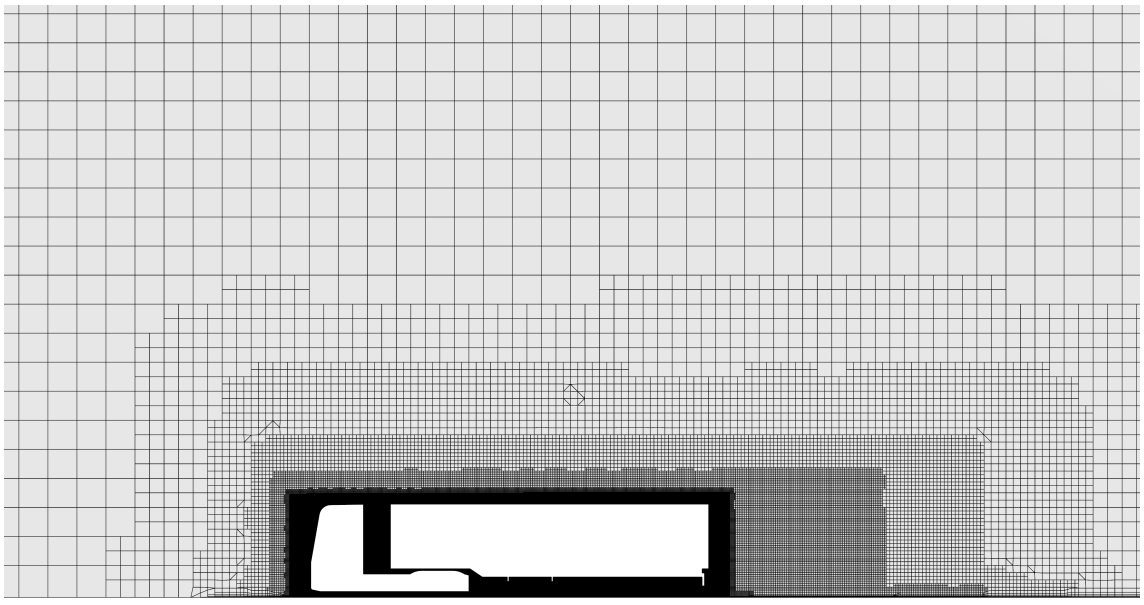

Figure 3.7: Illustration of the mesh refinement regions around the truck

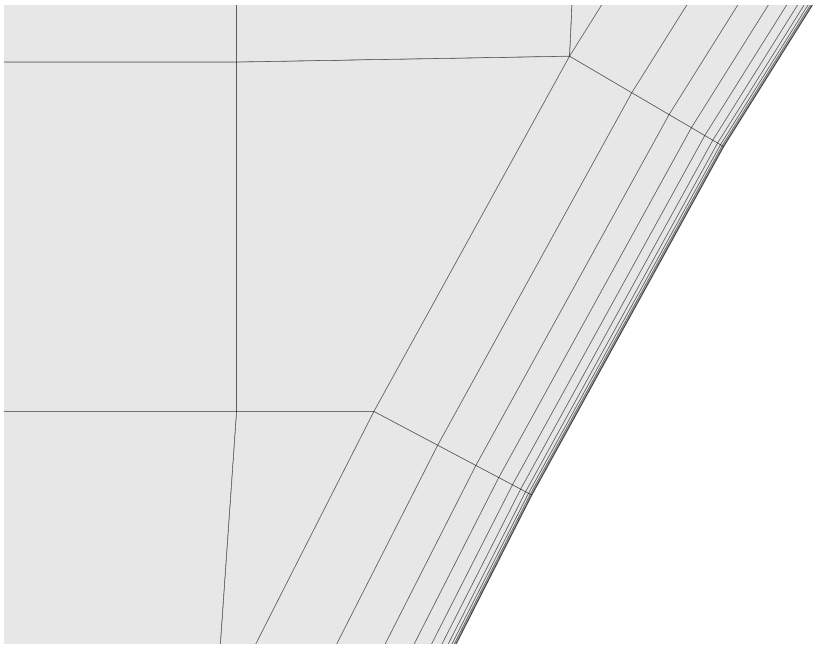

Figure 3.8: Prism cells near the truck surface

3.3 Optimization

3.3.1 SHERPA Algorithm

SHERPA (Simultaneous Hybrid Exploration that is Robust, Progressive, and Adaptive) is an optimization algorithm available in STAR-CCM+. In a single search, the algorithm uses multiple search methods simultaneously rather than sequentially. This approach uses the best attributes of each search method while reducing the participation of ineffective methods.

The algorithm also combines global and local search methods within the same optimization run. It explores a wide range of possible designs and then performs detailed refinement around the best candidates to efficiently obtain an optimal solution.

One optimization approach available in SHERPA is the weighted-sum approach. This approach can be used for both single-objective and multi-objective optimization problems. In the case of multiple objectives, a linear weighting is applied to combine the objectives into a single performance function that is subsequently optimized. The weighting factors determine the relative importance of each objective and allow trade-offs between competing performance metrics to be considered. For single-objective problems, the weighted-sum formulation reduces directly to the optimization of a selected objective.

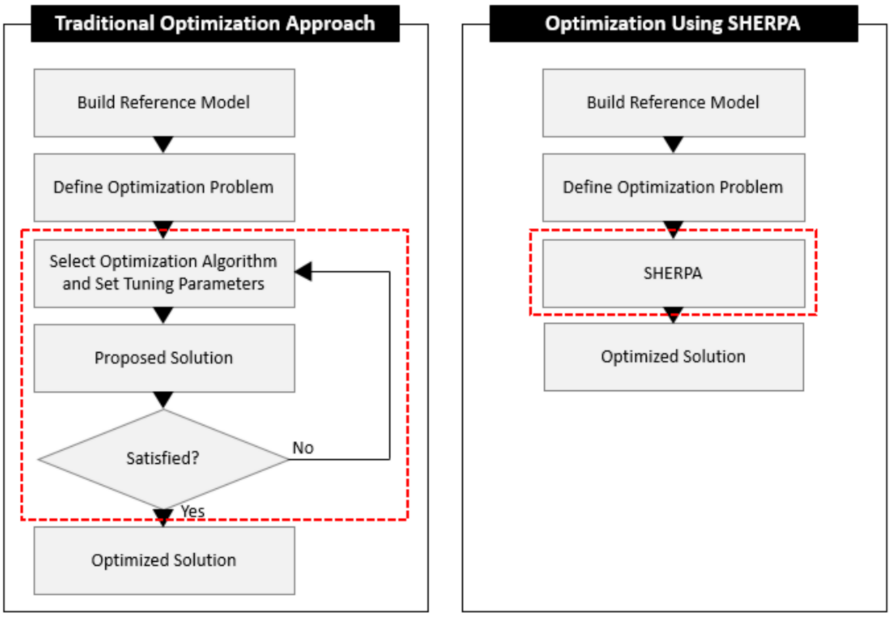

Figure 3.9: The SHERPA optimization flowchart

3.3.2 Optimization Setup

First, a design manager project was created. In the design manager project, a simulation file is selected as the reference model for the study. Then a design study was defined using an optimization study type, with simulation used as an evaluation method. A weighted-sum multi-objective optimization approach was applied. The drag coefficient (C_d) was chosen as the study response with the objective to reduce it, and 120 design runs were set to be performed.

Model 1, configuration 0, was used initially. This simplified model reduces computational time and has good convergence behavior. At this stage, only five of the eleven tractor parameters were included in the optimization. During the first three runs, the optimization did not perform as expected. This was attributed to the increment being either too large or too small. After several trials, it was found that setting the resolution to nine produced a suitable increment, resulting in normal optimization behavior.

After confirming that the optimization was running well, the complete version of Model 1 was used. The input parameters and their corresponding values used for the optimization are presented in Table 3.4.

Table 3.4: Design study input parameters

Parameter	Reference Value	Baseline Value	Range	Increment
RoofAngle (deg)	89	89	[70, 90]	1.25
SideAngle (deg)	5	5	[3.0, 12.5]	1.1875
WSAngle (deg)	80	80.0	[55.0, 80.0]	3.125
FenderAngle (deg)	10	10	[3.0, 12.5]	1.1875
BumperHeight (m)	1.25	1.25	[0.4, 1.25]	0.10625
FilletRadius (m)	0.2	0.2	[0.2, 0.5]	0.0375
RWSRadius (m)	0.5	0.5	[0.3, 2.0]	0.2125
FenderRadius (m)	0.2	0.2	[0.15, 1.3]	0.14375
BumperRadius (m)	0.2	0.2	[0.15, 0.75]	0.075
SideRadius (m)	0.215	0.215	[0.2, 0.3]	0.0125
Length (m)	2.26	2.26	[2.26, 3.26]	0.125

4

Add-on and Cab Geometry Effects

This chapter evaluates how the aerodynamic add-ons and cab geometry influence the drag of the complete tractor-trailer models. The discussion is based on the drag coefficient, accumulated drag coefficient, pressure coefficient contours, and velocity fields. Model 1 is first examined as the baseline cab geometry, followed by Model 2, which represents a more streamlined electric-truck cab. The final section compares the two models to identify the main aerodynamic mechanisms behind the observed differences.

4.1 Model 1

The aerodynamic results for Model 1 are summarized in Table 4.1. Configuration 1 is the reference case without the large side skirt or side extender. Adding the large side skirt in configuration 2 reduces C_d from 0.407 to 0.393, corresponding to a reduction of approximately 3.4%. Configuration 3, which combines the large side skirt with the side extender, gives the lowest drag coefficient for Model 1, with $C_d = 0.391$. This corresponds to an overall reduction of approximately 3.9% relative to the reference configuration.

Table 4.1: Results of Model 1

Model	**Configuration**	**Wheels**	**Large Side Skirt**	**Side Extender**	C_d
Model 1	Config. 1	x			0.407
Model 1	Config. 2	x	x		0.393
Model 1	Config. 3	x	x	x	0.391

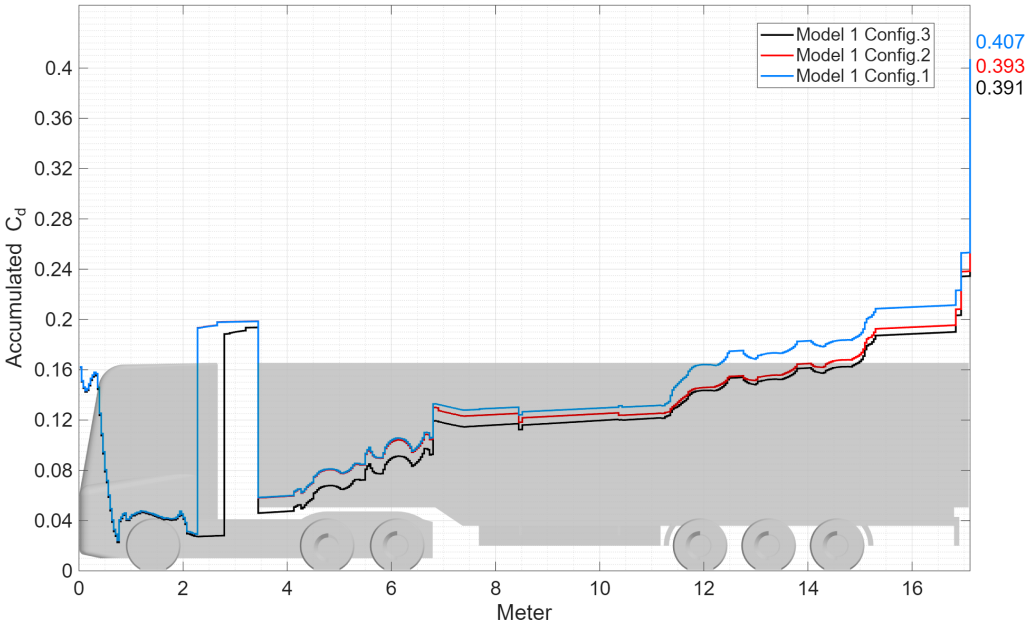

Figure 4.1: Accumulated C_d plot for Model 1

Figure 4.1 shows the accumulated drag coefficient along the length of Model 1 and helps identify the regions that dominate the total drag. The first increase occurs at the tractor front, where the incoming flow impinges on the flat cab surface and creates a high-pressure stagnation region. Because the tractor geometry is identical in all three Model 1 configurations, the front contribution is almost unchanged between the cases. Downstream of the stagnation region, the flow accelerates around the tractor corners and the pressure decreases, as shown in Figure 4.2a. This creates locally forward-directed pressure forces and causes a temporary decrease in accumulated C_d.

A second drag increase appears near the tractor-trailer gap. In the reference configuration, the flow separates from the rear of the tractor and enters the open gap, forming a recirculating low-pressure region. Figures 4.3a and 4.4a show the pressure loss at the tractor rear and the pressure loading on the trailer front. These pressure differences increase the drag contribution of the gap region. In configuration 3, the side extender reduces the effective gap opening and guides the flow more smoothly from the tractor toward the trailer. The pressure field becomes more uniform, and the low-pressure region at the tractor rear is reduced, as shown in Figures 4.3b and 4.4b. This explains the drag reduction obtained when the side extender is included.

Between approximately 4 m and 7 m, the wheels contribute to the accumulated drag by disturbing the near-ground flow. The rotating tires and wheel housings generate local separation, vortices, and wake structures, which increase momentum loss around the tractor and trailer underbody.

The trailer underbody is another important drag-producing region, especially between approximately 7 m and 15 m. In configuration 1, part of the external flow

enters the open underbody region and interacts with structural components, producing localized high-pressure areas beneath the trailer. This behavior is visible in Figures 4.5a and 4.5b. The large side skirt used in configurations 2 and 3 limits the amount of flow entering the underbody and keeps more of the flow attached along the outer side of the vehicle. As a result, the high-pressure regions beneath the trailer are reduced, as shown in Figure 4.6b, leading to a lower drag contribution from the underbody.

The final major drag increase occurs at the trailer base. At this location, the flow separates from the rear edges of the trailer and forms a large low-pressure wake. This base-wake contribution remains substantial for all Model 1 configurations because the rear trailer geometry is unchanged.

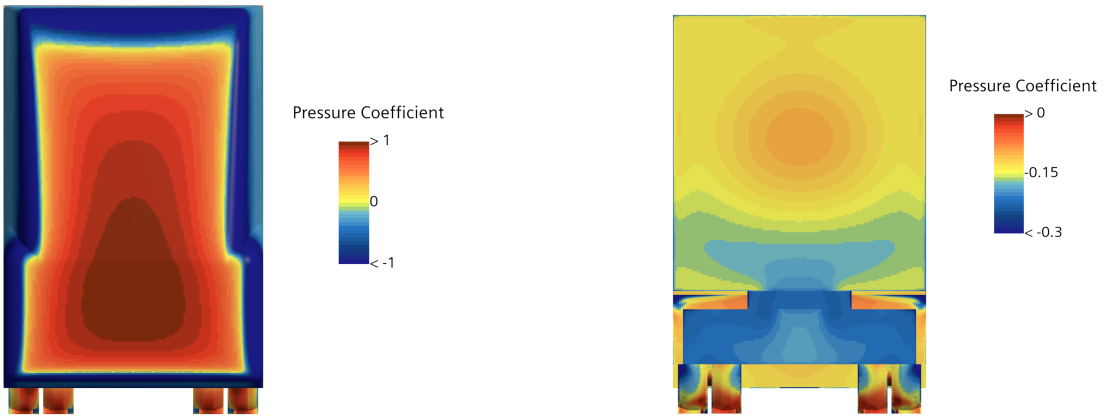

(a) Tractor front **(b)** Trailer back

Figure 4.2: Pressure coefficient of Model 1, configuration 1

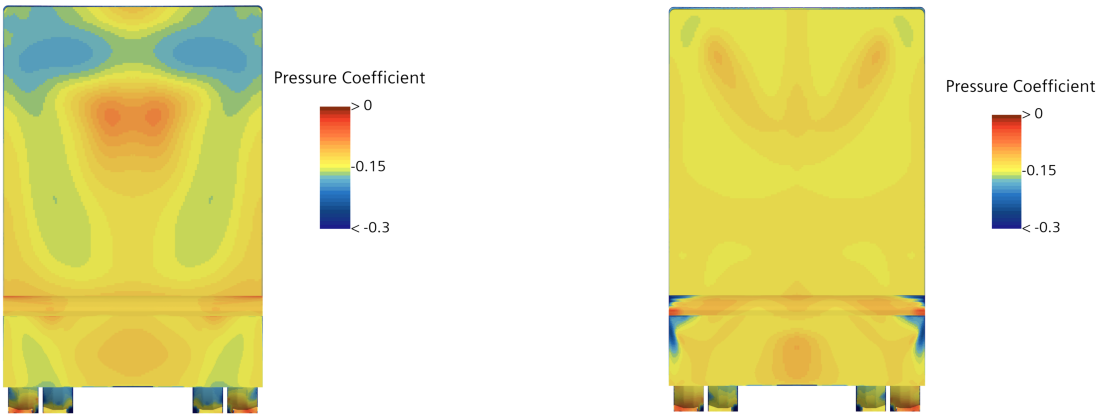

(a) Tractor back **(b)** Tractor back

Figure 4.3: Pressure coefficient of Model 1, configurations 1 and 3

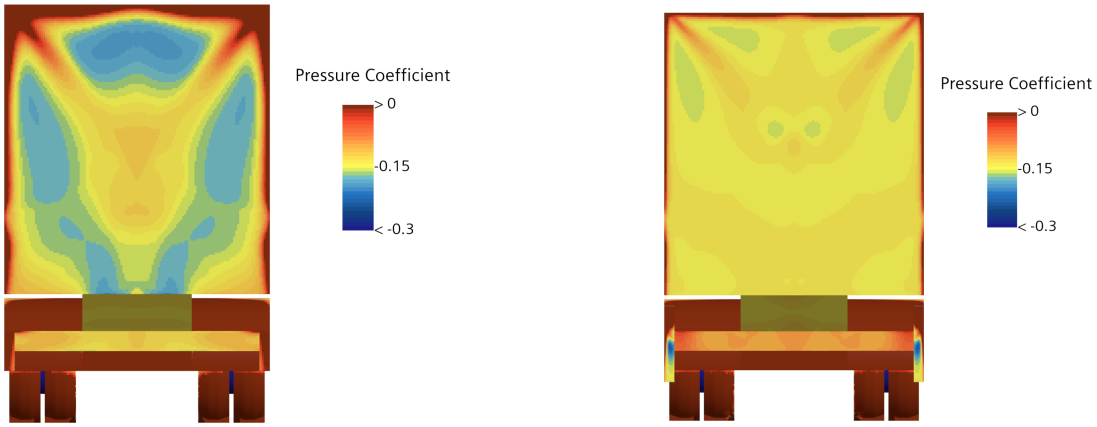

(a) Trailer front **(b)** Trailer front

Figure 4.4: Pressure coefficient of Model 1, configurations 1 and 3

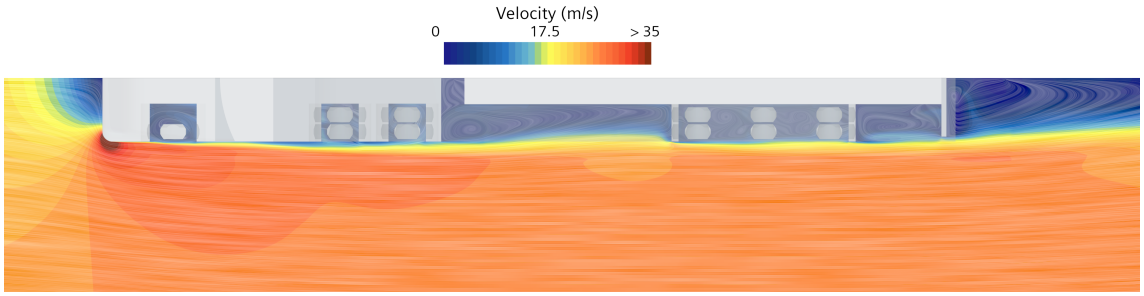

(a) Top view, configuration 1

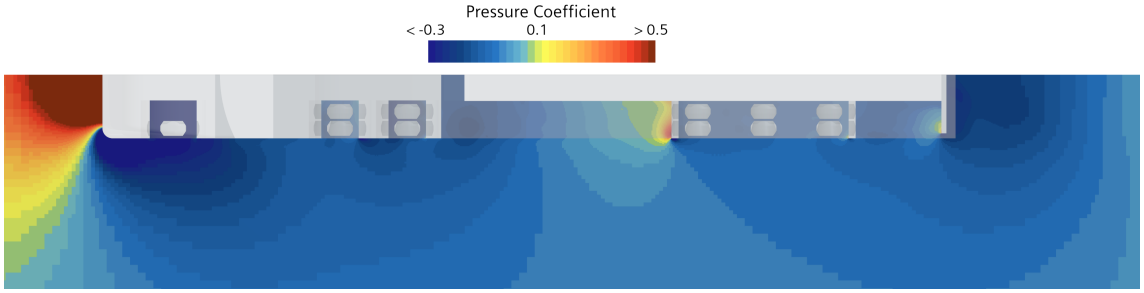

(b) Top view, configuration 1

Figure 4.5: Velocity contour and pressure coefficient at Z=0.7 m of Model 1

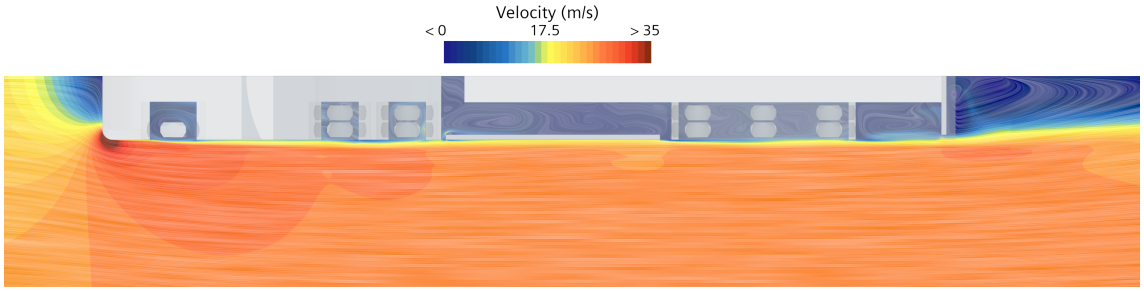

(a) Top view, configuration 3

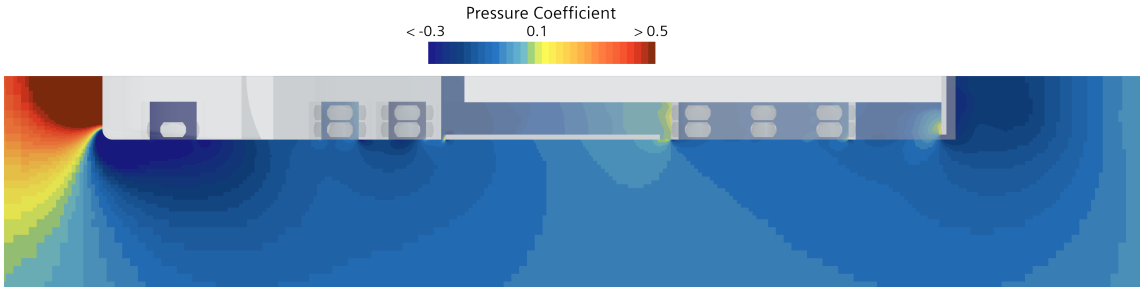

(b) Top view, configuration 3

Figure 4.6: Velocity contour and pressure coefficient at Z=0.7 m of Model 1

4.2 Model 2

The aerodynamic results for Model 2 are summarized in Table 4.2. As for Model 1, the add-on configurations reduce the drag compared with the reference case. The large side skirt in configuration 2 reduces C_d from 0.411 to 0.374, corresponding to a reduction of approximately 9.0%. Configuration 3 provides the lowest drag coefficient, with $C_d = 0.364$, which is approximately 11.4% lower than the Model 2 reference configuration.

Table 4.2: Results of Model 2

Model	**Configuration**	**Wheels**	**Large Side Skirt**	**Side Extender**	C_d
Model 2	Config. 1	x			0.411
Model 2	Config. 2	x	x		0.374
Model 2	Config. 3	x	x	x	0.364

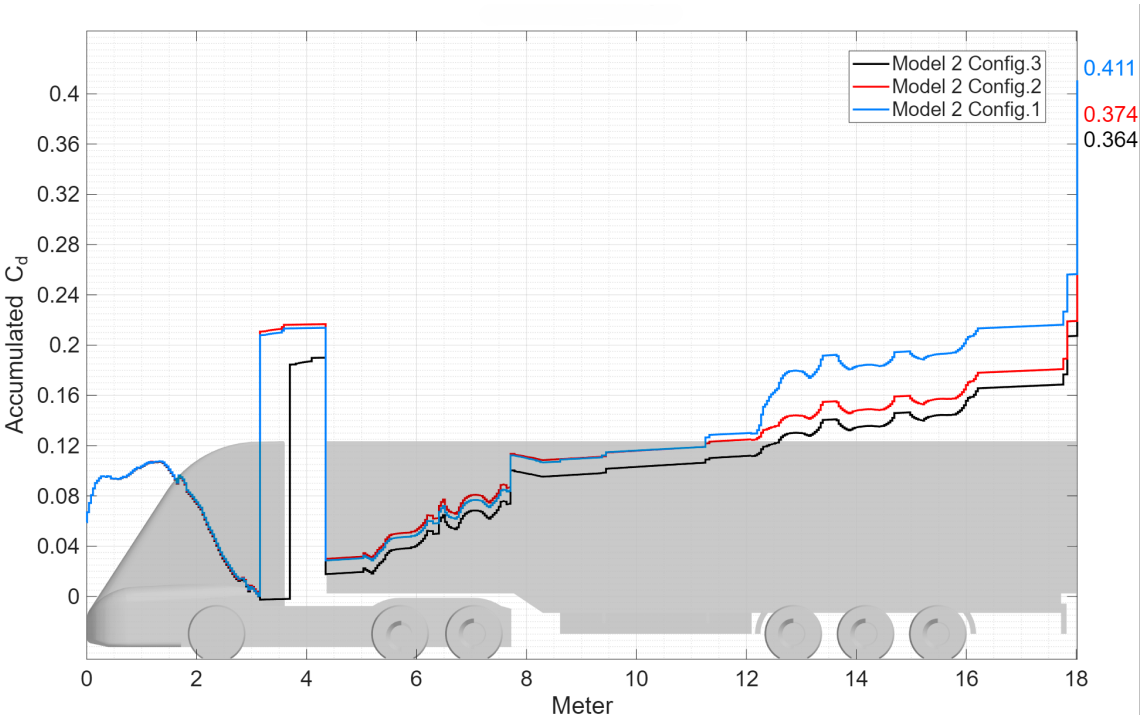

Figure 4.7: Accumulated C_d plot for Model 2

Figure 4.7 shows that the accumulated C_d trend for Model 2 is similar to that of Model 1, but the contributions are different along the vehicle. At the tractor front, Model 2 generates a lower drag contribution. This is caused by the reduced bumper height, smaller windshield angle, longer cab nose, and larger corner radii, which reduce the frontal area exposed normal to the incoming flow and promote smoother flow deflection around the cab. The lower pressure level on the tractor front is shown in Figure 4.8a.

In contrast, the tractor-trailer gap becomes more influential for Model 2, especially in configurations 1 and 2, where no side extender is installed. The pressure fields in Figures 4.9a and 4.10a show low-pressure regions in the gap, indicating separated and recirculating flow. This pressure loss increases the drag generated between the tractor and trailer. In configuration 3, the side extender reduces the open gap and improves pressure recovery, which explains the larger reduction in accumulated drag compared with configuration 1 and 2.

The wheel and underbody regions follow the same general trend as Model 1, but the reference configuration of Model 2 shows a stronger drag increase around the trailer underbody. Around 12 m, configuration 1 exhibits a steeper rise in accumulated C_d. Figure 4.11 indicates that more flow enters the underbody region, producing a localized high-pressure area near the wheel cover. When the large side skirt is added, as shown in Figure 4.12, this underbody flow is restricted and the pressure loading is reduced, contributing to the larger drag reduction observed for Model 2 configurations 2 and 3.

The final major drag increase occurs at the trailer base. At this location, the flow separates from the rear edges of the trailer and forms a large low-pressure wake. This base-wake contribution remains substantial for all Model 2 configurations because the rear trailer geometry is unchanged.

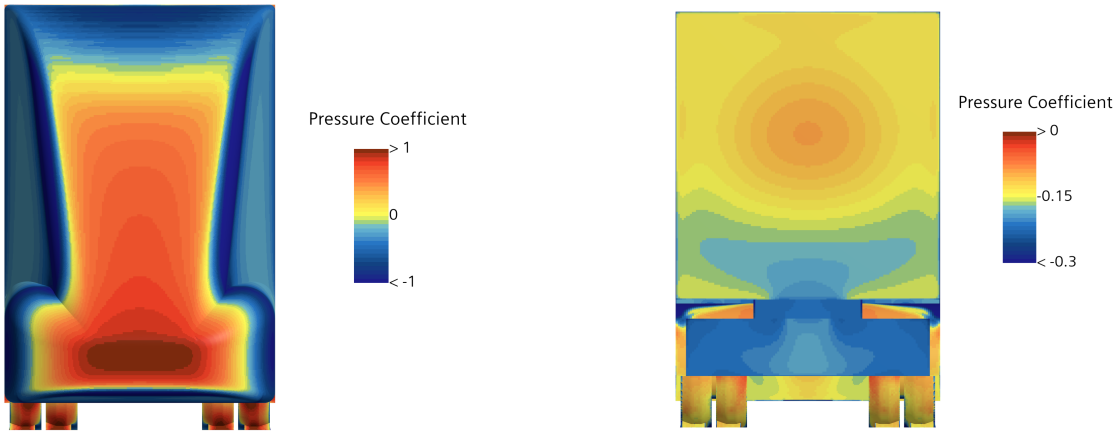

(a) Tractor front **(b)** Trailer back

Figure 4.8: Pressure coefficient of Model 2, configuration 1

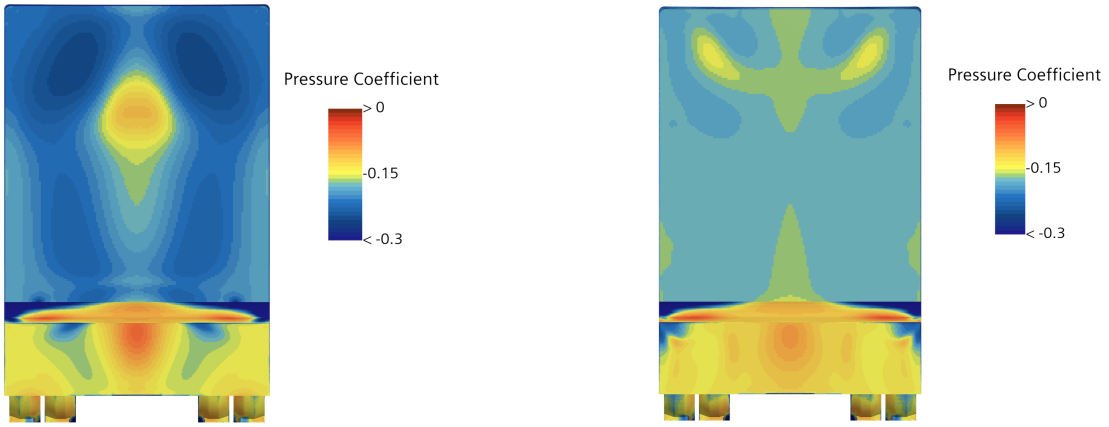

(a) Tractor back **(b)** Tractor back

Figure 4.9: Pressure coefficient of Model 2, configurations 1 and 3

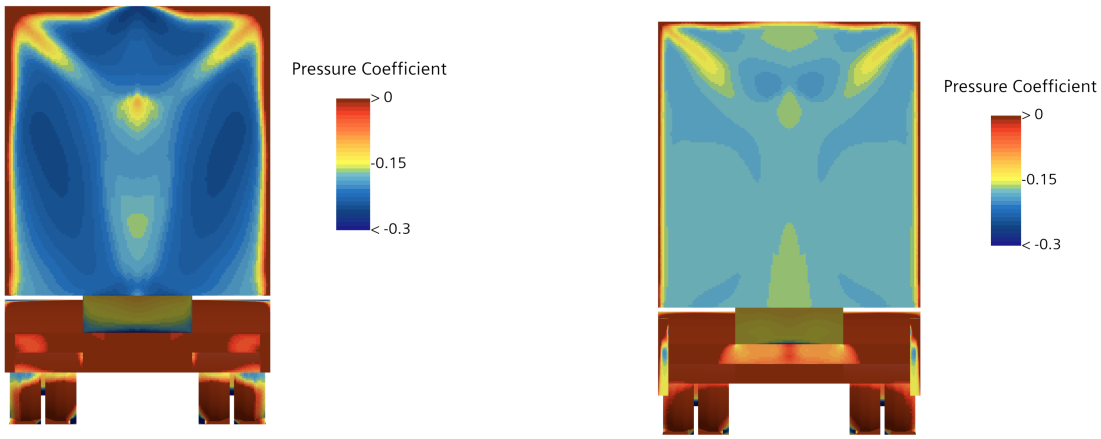

(a) Trailer front **(b)** Trailer front

Figure 4.10: Pressure coefficient of Model 2, configurations 1 and 3

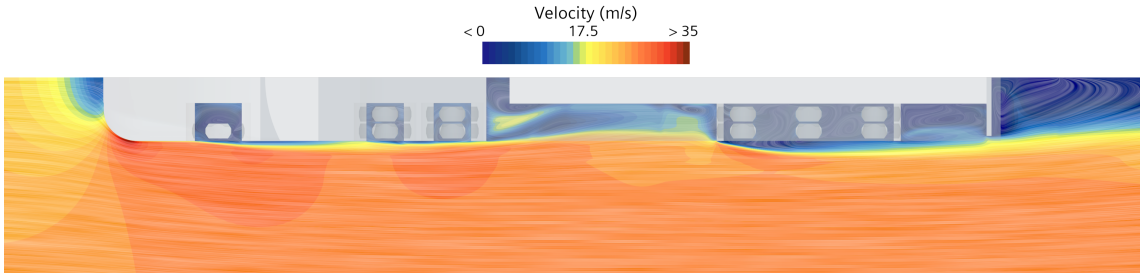

(a) Top view, configuration 1

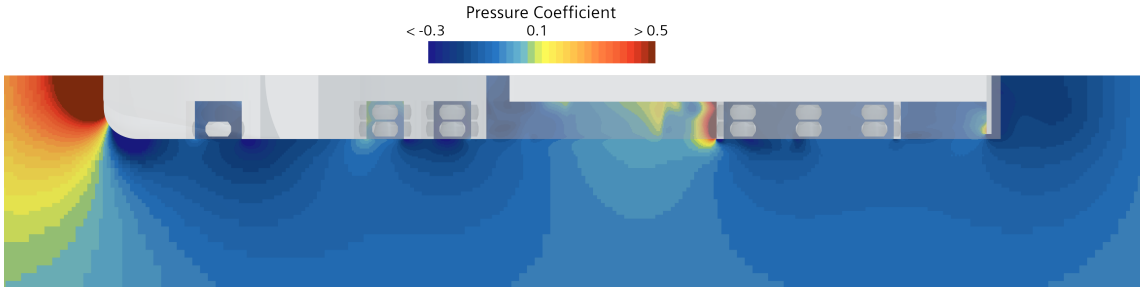

(b) Top view, configuration 1

Figure 4.11: Velocity contour and pressure coefficient at Z=0.7 m of Model 2

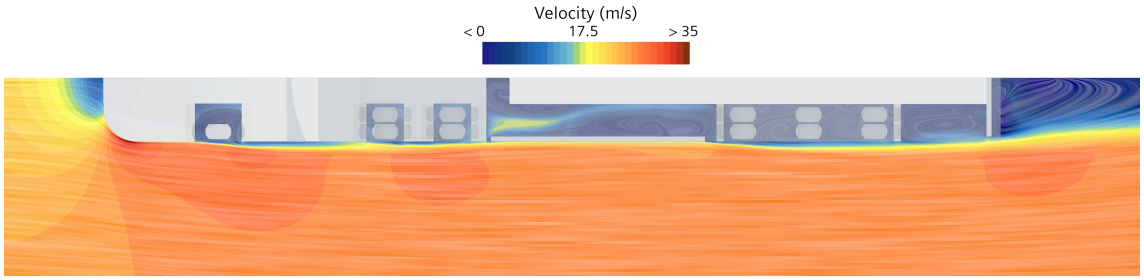

(a) Top view, configuration 3

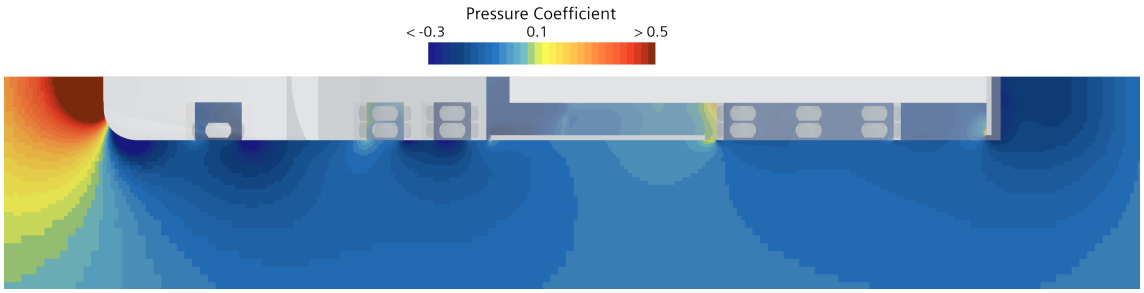

(b) Top view, configuration 3

Figure 4.12: Velocity contour and pressure coefficient at Z=0.7 m of Model 2

4.3 Comparison of Models

Table 4.3 summarizes the aerodynamic performance of all complete configurations. Without the large side skirt or side extender, Model 2 has a slightly higher total drag coefficient than Model 1, even though its cab front is more streamlined. This indicates that the benefit of reducing the frontal pressure drag can be offset by less favorable flow behavior downstream, particularly in the tractor-trailer gap and trailer underbody regions.

Table 4.3: Results summary of the models

Model	Configuration	Wheels	Large Side Skirt	Side Extender	C_d
Model 1	Config. 1	x			0.407
Model 1	Config. 2	x	x		0.393
Model 1	Config. 3	x	x	x	0.391
Model 2	Config. 1	x			0.411
Model 2	Config. 2	x	x		0.374
Model 2	Config. 3	x	x	x	0.364

The add-ons are more effective on Model 2 than on Model 1. For Model 1, the large side skirt reduces C_d by approximately 3.4%, while the combined side skirt and side extender reduce C_d by approximately 3.9%. For Model 2, the corresponding reductions are approximately 9.0% and 11.4%. The difference indicates that the streamlined cab geometry changes the downstream flow structure in a way that makes the gap and underbody treatments more important.

The pressure comparison in Figure 4.13 helps explain this behavior. Model 2 reduces the pressure on the tractor front because the smaller windshield angle, lower bumper height, and larger roof-windshield radius decrease the area facing the incoming flow and guide the flow more smoothly over the cab. However, this smoother front-end flow also shifts the separated flow development closer to the tractor-trailer gap. The gap pressure is therefore lower for Model 2, which increases the sensitivity of the complete vehicle to gap treatment.

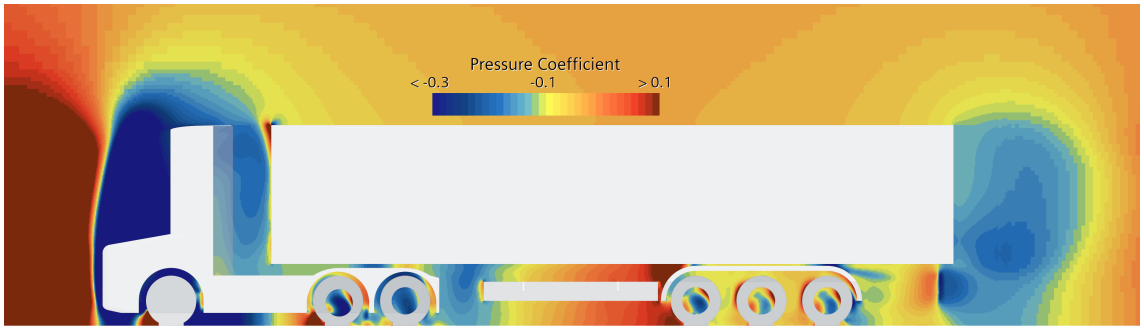

(a) Side view, configuration 1

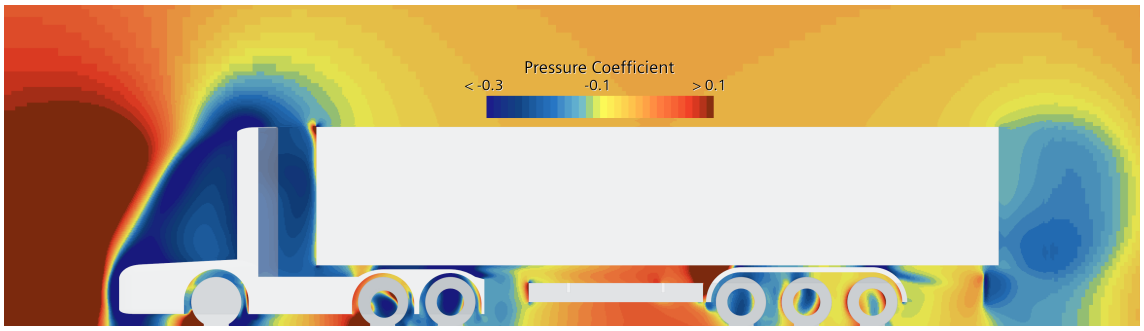

(b) Side view, configuration 1

Figure 4.13: Pressure coefficient at Y=-1.2 m of Model 1 and Model 2

The top-view comparison in Figure 4.14 shows that Model 2 also reduces separation around the tractor side corners because of the larger bumper, fillet, and side radii. This is beneficial locally, but it changes how flow is directed toward the trailer underbody. With less separation along the tractor sides, more energetic external flow can reach the lower trailer region and enter the underbody gaps, where it interacts with wheels and structural components. This explains why Model 2 can have a slightly higher drag coefficient in the reference configuration despite its improved cab-front pressure distribution.

When the large side skirt and side extender are installed, these downstream losses are reduced. The side extender improves pressure recovery in the tractor-trailer gap, while the side skirt blocks part of the flow entering the trailer underbody. As a result, Model 2 benefits more strongly from the add-ons than Model 1. This highlights an important design implication: a streamlined cab alone does not guarantee the lowest drag for a complete tractor-trailer vehicle. The aerodynamic performance depends on the interaction between the cab geometry, the tractor-trailer gap, the trailer underbody, and the add-on devices.

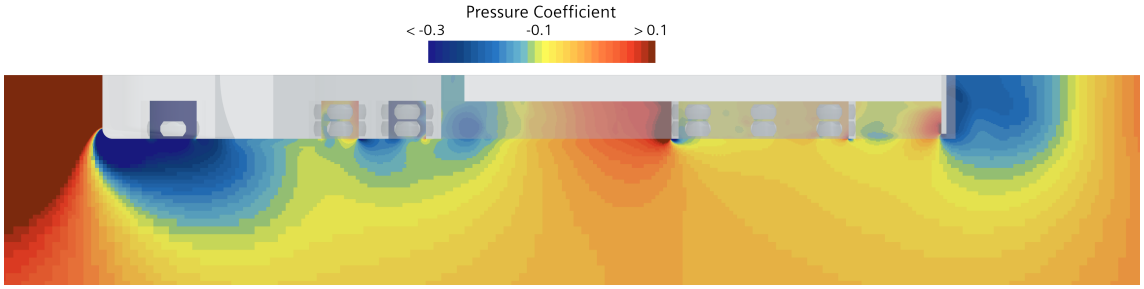

(a) Top view, configuration 1

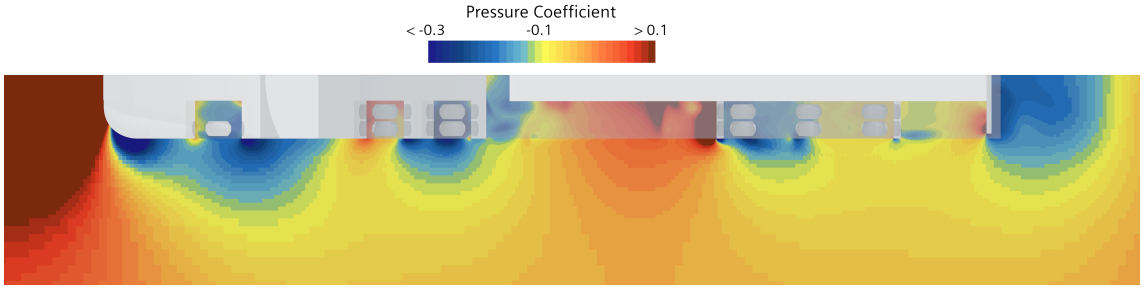

(b) Top view, configuration 1

Figure 4.14: Pressure coefficient at Z=0.7 m of Model 1 and Model 2

5

Cab Geometry Optimization

This chapter presents the cab-geometry optimization results. The optimization was carried out in two stages. First, a simplified version of Model 1, configuration 0, was used to verify the optimization setup and examine the response of selected cab parameters with reduced computational cost. The complete Model 1 geometry with aerodynamic add-ons was then optimized to evaluate the drag-reduction potential of the cab shape in the final vehicle configuration.

5.1 Simplified Model 1 Optimization

The simplified optimization case was based on Model 1, configuration 0. As shown in Figure 5.1, the SHERPA algorithm evaluated 95 designs and identified design 19 as the best-performing candidate.

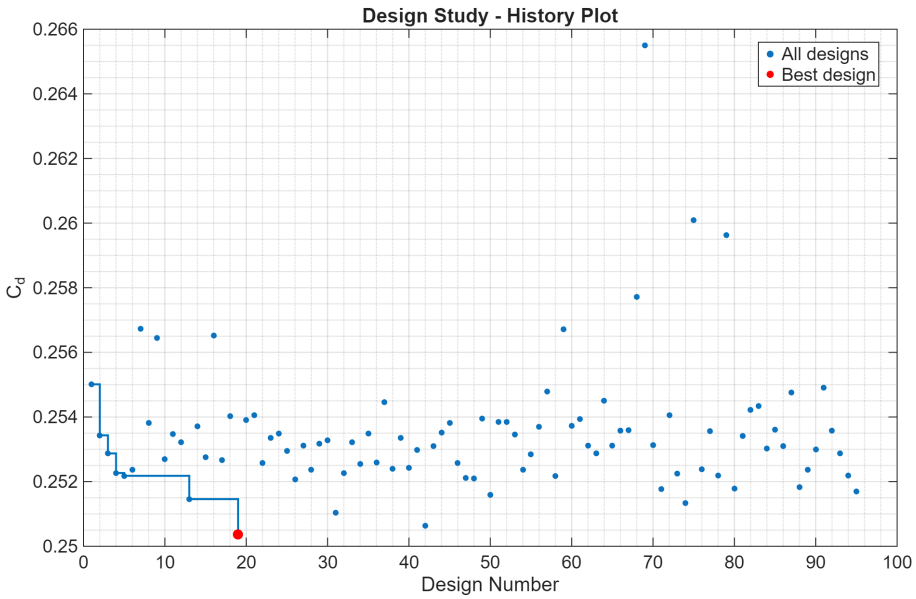

Figure 5.1: SHERPA search history for the simplified Model 1 optimization

Table 5.1 presents the optimized parameter values identified by the optimization algorithm as producing the lowest drag coefficient. As this is only a simplified model used for initial testing, only five parameters are optimized and presented. The rest of the parameters remain the same.

The aerodynamic performance of the optimized simplified model is summarized in Table 5.2. The drag coefficient is reduced from 0.259 to 0.250, corresponding to a reduction of approximately 3.5% relative to Model 1, configuration 0. Although this case does not include all vehicle details, it confirms that the selected cab parameters have a measurable influence on aerodynamic drag and provides a useful basis for the complete model optimization.

Table 5.1: Optimized cab parameters for the simplified Model 1 case

Parameter	Optimization Value	Reference Value
WSAngle (deg)	75.5	80
BumperHeight (m)	0.59	1.25
FilletRadius (m)	0.43	0.2
RWSRadius (m)	0.77	0.5
Length (m)	3	2.26

(a) Reference tractor **(b)** Optimized tractor

Figure 5.2: Front-view comparison for the simplified Model 1 optimization

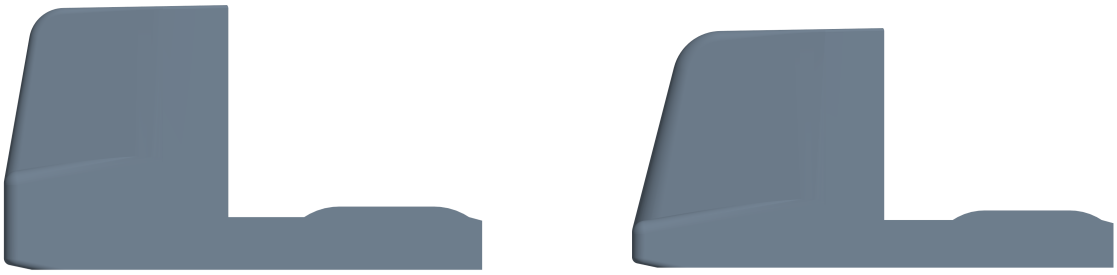

(a) Reference tractor **(b)** Optimized tractor

Figure 5.3: Side-view comparison for the simplified Model 1 optimization

Table 5.2: Aerodynamic result for the simplified Model 1 optimization

Model	Configuration	C_d
Model 1	Config. 0	0.259
Model 1	Optimized	0.250

5.2 Complete Model 1 Optimization

After the simplified study, the optimization was applied to the complete Model 1 configuration with wheels, the large side skirt, and the side extender. The search history is shown in Figure 5.4. In this stage, the SHERPA algorithm evaluated 120 designs and selected design 80 as the best-performing geometry.

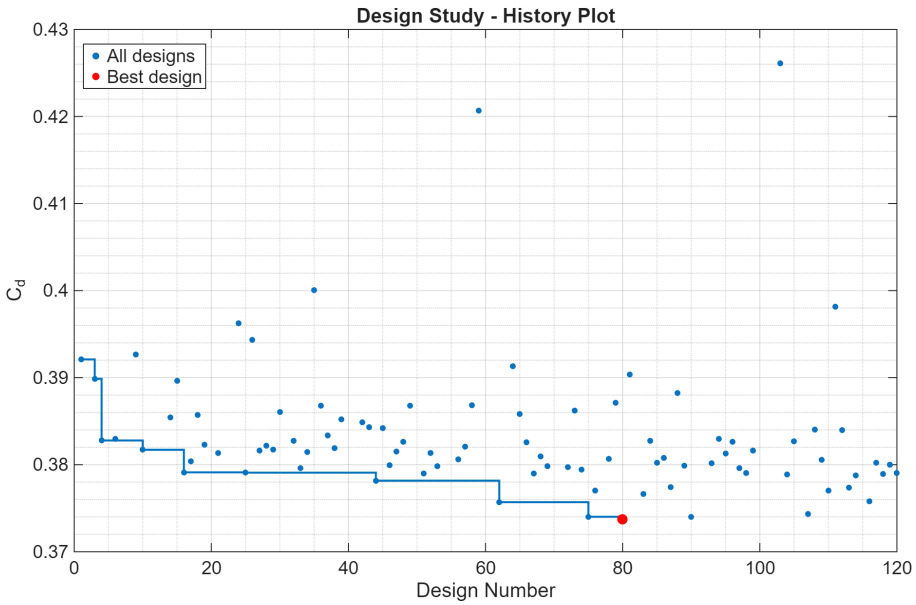

Figure 5.4: SHERPA search history for the complete Model 1 optimization

Table 5.3 presents the optimized parameter values for the complete Model 1 case. The final design again reduces the bumper height and windshield angle, while also slightly reducing the fender angle and increasing the cab length. The bumper radius, fillet radius, and fender radius are increased, which rounds the tractor front. These trends are consistent with the behavior observed for Model 2 in Chapter 4, where a more streamlined cab front produced a lower drag contribution. Figures 5.5b and 5.6b show the resulting front and side geometry of the optimized tractor.

Table 5.3: Optimized cab parameters for the complete Model 1 case

Parameter	Optimization Value	Reference Value
RoofAngle (deg)	89	89
SideAngle (deg)	5.75	5
WSAngle (deg)	76.875	80
FenderAngle (deg)	8.9375	10
BumperHeight (m)	0.4	1.25
FilletRadius (m)	0.3125	0.2
RWSRadius (m)	0.3	0.5
FenderRadius (m)	0.4375	0.2
BumperRadius (m)	0.375	0.2
SideRadius (m)	0.215	0.215
Length (m)	2.76	2.26

(a) Reference tractor **(b)** Optimized tractor

Figure 5.5: Front-view comparison for the complete Model 1 optimization

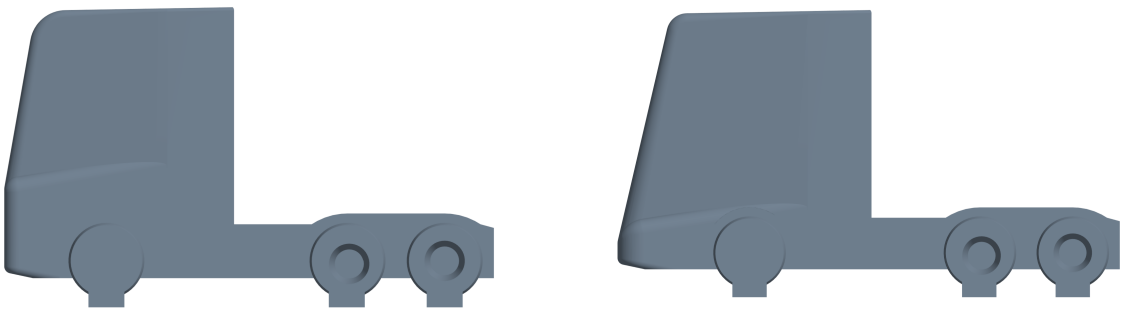

(a) Reference tractor **(b)** Optimized tractor

Figure 5.6: Side-view comparison for the complete Model 1 optimization

Table 5.4 compares the aerodynamic performance of the optimized model with Model 1, configuration 3. Both configurations include the same wheels, large side skirt, and side extender, so the difference in drag is mainly caused by the optimized cab geometry. The drag coefficient is reduced from 0.391 to 0.373, corresponding to a reduction of approximately 4.6%.

Table 5.4: Aerodynamic result for the complete Model 1 optimization

Model	**Configuration**	**Wheels**	**Large Side Skirt**	**Side Extender**	C_d
Model 1	Config. 3	x	x	x	0.391
Model 1	Optimized	x	x	x	0.373

The accumulated drag coefficient in Figure 5.7 shows that the main difference between the optimized model and Model 1, configuration 3, occurs at the tractor front. The optimized model has a lower front drag contribution, after which the two curves follow nearly identical trends. This indicates that the optimization mainly improves the cab front, while the downstream behavior remains similar because the add-ons, wheels, trailer geometry, and tractor-trailer gap treatment are unchanged.

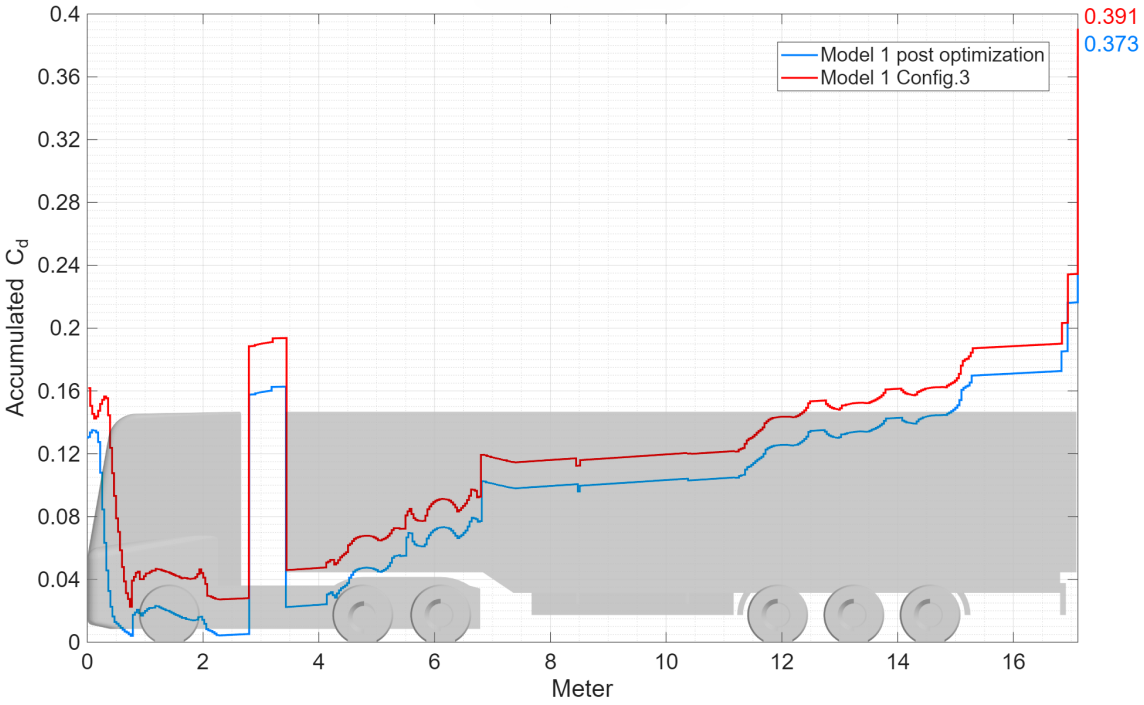

Figure 5.7: Accumulated C_d for Model 1 configuration 3 and the optimized model

The pressure coefficient comparisons in Figures 5.8–5.10 support the trend observed in the accumulated drag plot. At the tractor front, the optimized model reduces the

extent of the high-pressure region and produces a smoother pressure distribution over the cab surface. At the tractor back and trailer front, the pressure fields remain broadly similar between the two configurations. This confirms that the drag reduction is primarily obtained from the optimized cab front shape, rather than from a major change in the tractor-trailer gap flow.

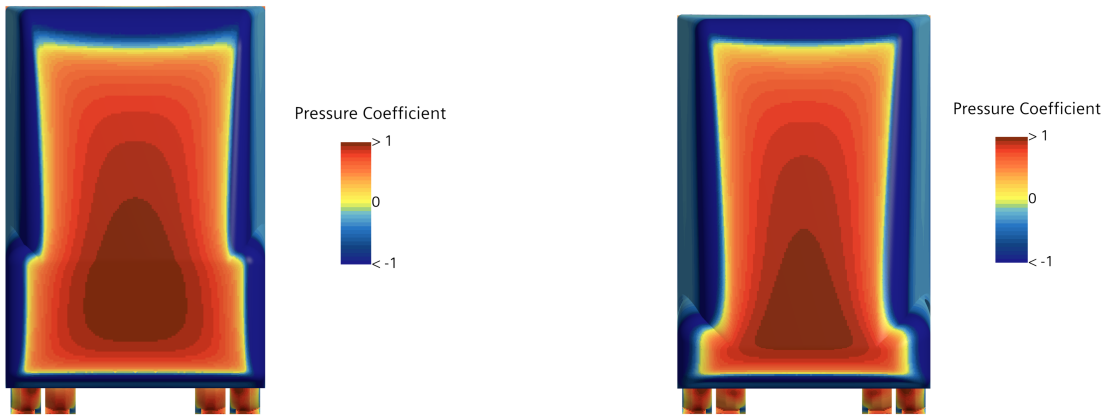

(a) Tractor front, configuration 3 **(b)** Tractor front, optimized

Figure 5.8: Pressure coefficient for Model 1 configuration 3 and the optimized model

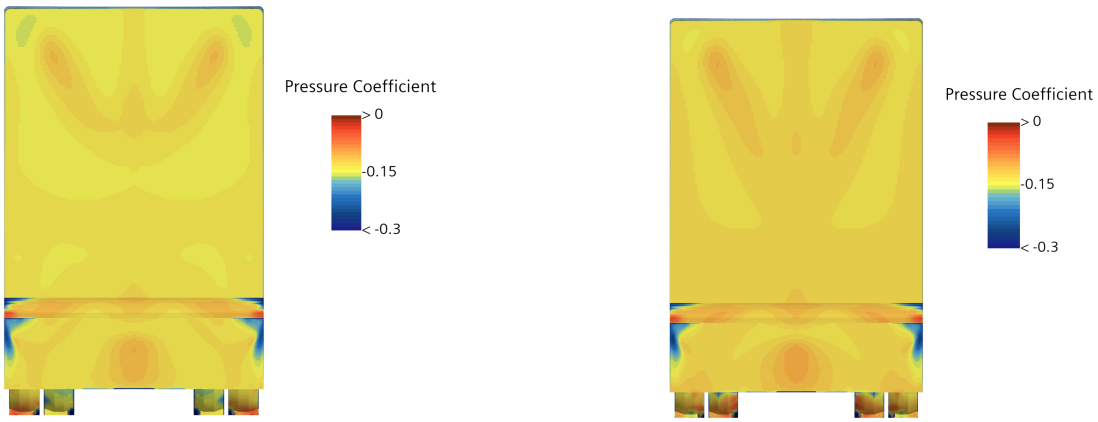

(a) Tractor back, configuration 3 **(b)** Tractor back, optimized

Figure 5.9: Pressure coefficient for Model 1 configuration 3 and the optimized model

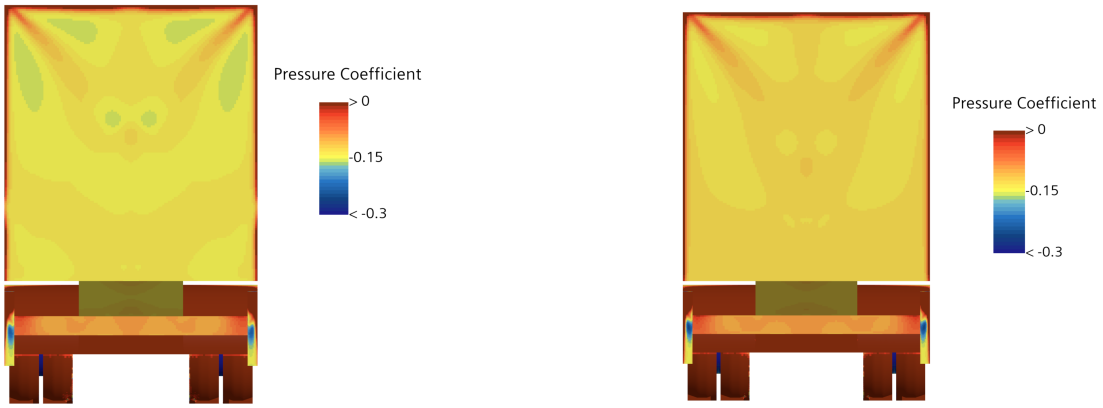

(a) Trailer front, configuration 3 **(b)** Trailer front, optimized

Figure 5.10: Pressure coefficient for Model 1 configuration 3 and the optimized model

Figure 5.11 shows the top-view velocity and pressure fields of the optimized complete model at $Z = 0.7$ m. The velocity contour indicates that the flow is redirected smoothly around the rounded cab front and then accelerates along the tractor sides. The pressure field shows the remaining stagnation region at the cab nose, followed by lower pressure along the side surfaces and through the tractor-trailer gap. This flow pattern is consistent with the optimized geometry: the front pressure load is reduced, while the downstream flow structure is still governed by the side extender, side skirt, and trailer arrangement.

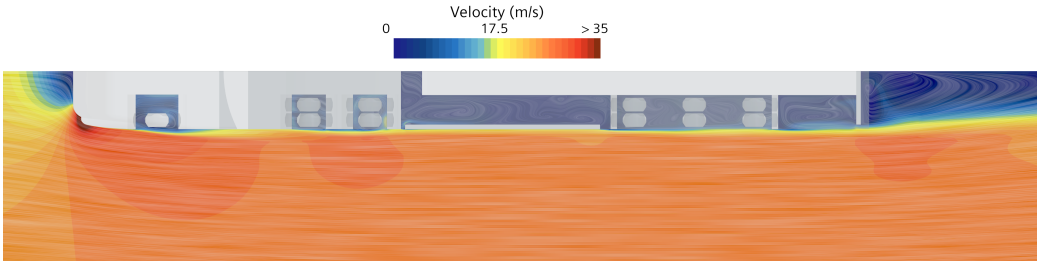

(a) Top view

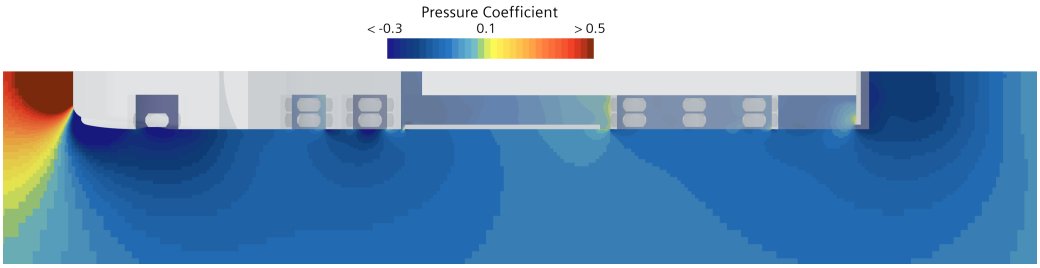

(b) Top view

Figure 5.11: Velocity contour and pressure coefficient of the optimized model at $Z = 0.7$ m

6

Conclusion

This project had three primary objectives. The first objective was to design and parameterize a 3D CAD model of a reference electric truck. Conduct CFD simulations on the model to assess the impact of selected aerodynamic design features, including cab geometry and aerodynamic add-ons such as side extenders and side skirts, on the aerodynamic drag of the truck. The third objective was to perform cab geometry optimization using the SHERPA algorithm with the objective of reducing aerodynamic drag.

A reference 3D electric truck was designed and parameterized in STAR-CCM+. Two different cab geometries with seven different configurations were investigated to assess their effect on the aerodynamic performance of the vehicle. It was observed that cab geometry plays a significant role in reducing aerodynamic drag. A more rounded and streamlined cab design promotes smoother flow deflection and reduces pressure drag by minimizing pressure and flow separation at the front of the truck.

The results show that cab geometry has a strong influence on both the front pressure distribution and the effectiveness of the add-ons. For Model 1, the combined large side skirt and side extender reduced the drag coefficient from 0.407 to 0.391, corresponding to a reduction of approximately 3.9%. For the more streamlined Model 2, the same add-on configuration reduced the drag coefficient from 0.411 to 0.364, corresponding to a reduction of approximately 11.4%. The complete Model 1 optimization reduced the drag coefficient from 0.391 to 0.373, giving an additional reduction of approximately 4.6% relative to Model 1 configuration 3. The accumulated drag and pressure-coefficient results indicate that this improvement mainly originates from the optimized cab-front shape, while the downstream flow remains strongly affected by the side skirt, side extender, and trailer arrangement.

In conclusion, optimizing cab geometry and implementing aerodynamic add-ons were found to be effective strategies for reducing aerodynamic drag in electric heavy-duty trucks. However, maximizing aerodynamic performance requires a comprehensive approach that considers the combined effects of tractor design, trailer geometry, and aerodynamic add-ons.

6.1 Further Studies and Improvements

In this study, multiple opportunities for further work and improvement have been identified.

Including validation through wind tunnel testing would provide experimental verification and improve the reliability of the results. Combining experimental measurement with numerical simulation would enable a more comprehensive evaluation of the investigated truck configurations.

The simulations in this study were limited to a yaw angle of 0°. Investigating different yaw angles would provide a more realistic representation of operating conditions and allow the influence of crosswinds on side forces, vehicle stability, and overall aerodynamic performance to be assessed.

The CFD simulation used Reynolds-Averaged Navier–Stokes turbulence modeling. Future work could investigate the use of Improved Delayed Detached Eddy Simulation (IDDES), which has the potential to capture more complex unsteady flow structures and wake dynamics. This would provide insight into the accuracy and limitations of the applied approach.

Finally, the optimization scope could be expanded. The present optimization focused on cab geometry, while the trailer, side skirt, side extender, and gap configuration were kept fixed. Future optimization studies could include these components as design variables and consider multi-objective targets such as drag, lift, side force, manufacturability, and packaging constraints. This would provide a more complete design framework for aerodynamic development of zero-emission heavy-duty vehicles.

Bibliography

[1] Brian R. McAuliffe, Faegheh Ghorbanishohrat, and Hali Barber. Preliminary investigation towards next generation truck design for aerodynamic efficiency. Laboratory Technical Report LTR-AL-2022-0069, National Research Council Canada, 2022.

[2] Niles Timmermans. Council sets position on maximum weights and dimensions for road vehicles - consilium, Dec 2025.

[3] J. Patten, B. McAuliffe, W. Mayda, and B. Tanguay. Review of aerodynamic drag reduction devices for heavy trucks and buses. Technical Report CSTT-HVC-TR-205, National Research Council Canada, 2012.

[4] European Commission. Road transport. EU Climate Action, 2026.

[5] European Commission. Lorries, buses and coaches. EU Climate Action, 2026.

[6] Bruce L. Storms, Dale R. Satran, James T. Heineck, and Stephen M. Walker. A summary of the experimental results for a generic tractor-trailer in the ames research center 7- by 10-foot and 12-foot wind tunnels. NASA Technical Memorandum NASA/TM-2006-213489, NASA Ames Research Center, 2006.

[7] K. Sreenivas, B. Mitchell, S. Nichols, D. Hyams, and D. Whitfield. Computational simulation of the gcm tractor-trailer configuration. In Fred Browand, Rose McCallen, and James Ross, editors, *The Aerodynamics of Heavy Vehicles II: Trucks, Buses, and Trains*, pages 325–338. Springer Berlin Heidelberg, Berlin, Heidelberg, 2009.

[8] Bruce L. Storms, James C. Ross, James T. Heineck, Stephen M. Walker, David M. Driver, and Gregory G. Zilliac. An experimental study of the ground transportation system (gts) model in the nasa ames 7- by 10-ft wind tunnel. NASA Technical Memorandum NASA/TM-2001-209621, NASA Ames Research Center, 2001.

[9] Christopher Roy, Jeffrey Payne, Mary McWherter-Payne, and Kambiz Salari. Rans simulations of a simplified tractor/trailer geometry. In Rose McCallen, Fred Browand, and James Ross, editors, *The Aerodynamics of Heavy Vehicles: Trucks, Buses, and Trains*, pages 207–218, Berlin, Heidelberg, 2004. Springer Berlin Heidelberg.

[10] Christopher J. Roy and Harshavardhan A. Ghuge. Detached eddy simulations of a simplified tractor/trailer geometry. In Fred Browand, Rose McCallen, and

James Ross, editors, *The Aerodynamics of Heavy Vehicles II: Trucks, Buses, and Trains*, pages 363–381. Springer Berlin Heidelberg, Berlin, Heidelberg, 2009.

[11] Kevin R. Cooper. Commercial vehicle aerodynamic drag reduction: Historical perspective as a guide. In Rose McCallen, Fred Browand, and James Ross, editors, *The Aerodynamics of Heavy Vehicles: Trucks, Buses, and Trains*, pages 9–28, Berlin, Heidelberg, 2004. Springer Berlin Heidelberg.

[12] Michael Gerard Connolly, Alojz Ivankovic, and Malachy J. O'Rourke. Drag reduction technology and devices for road vehicles - a comprehensive review. *Heliyon*, 10(13):e33757, 2024.

[13] Jeong Jae Kim, Jeongju Kim, and Sang Joon Lee. Substantial drag reduction of a tractor-trailer vehicle using gap fairings. *Journal of Wind Engineering and Industrial Aerodynamics*, 171:93–100, 2017.

[14] Bae Geun Hwang, Sangseung Lee, Eui Jae Lee, Jeong Jae Kim, Myeongkyun Kim, Donghyun You, and Sang Joon Lee. Reduction of drag in heavy vehicles with two different types of advanced side skirts. *Journal of Wind Engineering and Industrial Aerodynamics*, 155:36–46, 2016.

[15] J. Ortega, K. Salari, A. Brown, and R. Schoon. Aerodynamic drag reduction of class 8 heavy vehicles: A full-scale wind tunnel study. Technical Report LLNL-TR-628153, Lawrence Livermore National Laboratory, Livermore, CA, March 2013.

[16] Madhav S. Prabhu, Sudheendra Prabhu K, Amar A. Murthy, and Srinivas G. Aerodynamic drag reduction in commercial vehicle using CFD-based design optimisation. *F1000Research*, 14:821, August 2025.

[17] Mohd Hafiz Zawawi, A Saleha, A Salwa, NH Hassan, Nazirul Mubin Zahari, Mohd Zakwan Ramli, and Zakaria Che Muda. A review: Fundamentals of computational fluid dynamics (cfd). In *AIP conference proceedings*, volume 2030, page 020252. AIP Publishing LLC, 2018.

[18] Florian R. Menter. Two-equation eddy-viscosity turbulence models for engineering applications. *AIAA Journal*, 32(8):1598–1605, 1994.

DEPARTMENT OF MECHANICS AND MARITIME SCIENCES
CHALMERS UNIVERSITY OF TECHNOLOGY
Gothenburg, Sweden
www.chalmers.se

CHALMERS
UNIVERSITY OF TECHNOLOGY